Poly(Ethylene Terephthalate) Melt Spinning Via Controlled Threadline Dynamics

CHON-YIE LIN,* PAUL A. TUCKER, and JOHN A. CUCULO

Fiber and Polymer Science Program, North Carolina State University, Raleigh, North Carolina 27695-8301

SYNOPSIS

Fiber melt spinning of poly(ethylene terephthalate) (PET) was studied via modification of threadline dynamics. Several techniques were implemented in the high-speed spinning process for the judicious control of threadline dynamics. This included a thermal conditioning zone (TCZ) for controlling the threadline temperature profile and a hydraulic drag bath (HDB) for controlling the threadline spinning stress. Through controlled threadline dynamics, key factors affecting the structure development—namely, temperature, tensile stress, and crystallization time—were manipulated to favor formation of a highly oriented and transversely uniform structure in the spun fibers. This carries the implication that optimum or near-optimum processing conditions are being applied during the structure development period. More specifically, tensile stress in the threadline, independent of temperature, is substantially increased to many orders higher than that ordinarily attained in the normal high-speed spinning process. Concurrently, the temperature crucial to the structure development is being independently optimized and its duration extended to attain a highly oriented structural order. Properties of the spun fibers were found to be correlated with the threadline parameters including cooling profile, tension profile, and strain rate. PET fibers spun via the one-step process with the introduction of the TCZ and HDB possess superior mechanical performance. Structural characterization suggests that the spun fibers have a high amorphous orientation factor and a uniform radial structure distribution. Further on-line studies indicate that structure development in the threadline is completely different from that of the traditional high-speed spinning process. The attenuation profile of the threadline is observed to be dependent on TCZ temperature, residence time in the HDB, temperature of the HDB, and take-up speed. It is believed that for the melt spinning process with the TCZ and the HDB, the threadline dynamics is changed from one controlled by inertia and air drag forces to one controlled by the imposed hydraulic drag.

INTRODUCTION

Since the first synthesis of high polymers by Carothers and Hill,[1] the importance of spinning conditions on fiber structure was realized by polymer researchers; and hence techniques have been developed and continuously improved for making fibers from polymers including the wet, dry, and melt spinning processes to produce fibers with a wide range of properties. Of the three different spinning techniques, the melt process, without the added complexities of chemical reaction and/or mass transfer, is the simplest conceptually and economically for producing fibers suitable for textile and industrial end uses. Therefore, studies on structure development and its relation to spinning conditions during the melt spinning process have received much attention by researchers in attempts to understand the fundamental aspects of fiber formation. A main subject is to discover techniques for improving the properties of spun fibers. The polymer of current interest is poly(ethylene terephthalate) (PET), and its properties depend greatly on the spinning process

* To whom correspondence should be addressed.

Present address: Allied-Signal Inc., Technical Center, P.O. Box 31, Petersburg, VA 23804.

Journal of Applied Polymer Science, Vol. 46, 531–552 (1992)
 CCC 0021-8995/92/030531-22$04.00

conditions. Under most low and moderate spinning speeds as reported by Ziabicki and Kedzierska,[2] Dumbleton,[3] and Nakamura et al.,[4] PET exhibits very little or no crystallinity, and a separate drawing operation is essential to impart properties required for useful applications. In the late 1970s, studies by Shimizu et al.,[5] Heuvel and Huisman,[6] and Perez and Lecluse[7] indicated that PET fibers spun at 5000–6000 m/min exhibited a high degree of crystallinity, comparable to that of drawn fibers. Since that time research on the development of structure and mechanical properties in the high-speed threadline have been the center of interest of both academic and industrial laboratories[8] because of its potentially high technical feasibility and commercial appeal. In the melt spinning of PET fibers at take-up speeds above 4000 m/min, the crystallization starts to occur at a certain position in the threadline, where the filament is under high tensile stress as a result of the increasing inertia and air drag forces at high take-up speed. In spite of the high degree of crystallinity, fibers spun at high speed still possess a very low amorphous orientation, which results in a poor mechanical performance compared with those of the conventional low speed spun with subsequent drawing process. At further increase of spinning speed above 7000 m/min, the filament temperature falls rapidly due to the extremely high cooling rate. This implies that the residence time of the filament in the zone of maximum crystallization rate becomes shorter. The relatively short residence time of the filament in the zone of maximum crystallization rate consequently results in a lower level of crystallinity in ultra-high take-up speed. Moreover, severe radial structural variation occurs in the cross section of fiber spun at high speed due to the rapid cooling of filaments. Being aware of these problems in spinning fibers at high speeds, attempts were made to modify the threadline via control of the threadline dynamics in terms of temperature and stress profiles. Experimental results of modifying threadline dynamics with a combination of on-line zone cooling and heating have been reported by Cuculo et al.[9,10] showing a significant improvement of molecular orientation, crystallinity, and mechanical properties of the resulting fibers. In this study the temperature profile of the high-speed threadline was modified by the judicious control of the surrounding temperature aimed to delay cooling and consequently to extend the crystallization time for the enhancement of structure formation. In addition, a technique was implemented in the high-speed spinning process for the control of take-up stress. Through controlled threadline dynamics, key factors affecting the structure development—namely, temperature, tensile stress, and crystallization time—were manipulated to favor formation of a highly oriented morphology and a superior radial uniformity of spun fibers.

EXPERIMENTAL

Spinning Process

Poly(ethylene terephthalate) resins used in this study were supplied by the Goodyear Tire and Rubber Company. Characterization of PET resins reveals intrinsic viscosity (IV) of 0.95 dL/g and number-average molecular weight of 36,615. Prior to spinning, PET chips were dried in a vacuum oven at 140°C for at least 14 h. To prepare for a spinning run, the extruder and spinning block were heated for approximately 3 h to attain thermal stability. A typical run began by loading the dried PET chips into the nitrogen-purged hopper. In the extrusion process the spinning block was set at 305°C as the spinning temperature. A hyperbolic spinneret with a round orifice having a 0.6 mm diameter, as stated by Ihm and Cuculo,[11] was employed in this work. Unless otherwise stated, the mass flow rate per orifice was adjusted to produce a linear density of 5.0 denier per filament. A thermal conditioning zone (TCZ) of 13 cm length and 8.1 cm inside diameter was used, and it provided radial inflow hot air at up to 250°C and 120 ft/min flow rate. It was placed in the threadline with a 10-cm gap between the face of the spinneret and the top of the heating chamber. Temperature profile of the high-speed threadline was thus modified by the judicious control of the surrounding temperature. The essential part of the stress-enhancing apparatus was conducted via a hydraulic drag bath (HDB). The HDB in the threadline was placed such that the surface of the liquid was 420 cm from the face of the spinneret and 150 cm from the take-up roll as shown in Figure 1. The liquid medium used in this study was water at 25°C and 95°C, respectively, and 1,2-propanediol at 110°C and above. As illustrated in Figure 1, the threadline is passed downward and then upward through the HDB. Therefore, the total path length of threadline through the HDB, in such an arrangement being on the order of about two times the depth of the drag bath, was controllable from 1 to 32 cm. In operation, the height and temperature of the liquid medium in the HDB was maintained with an auxiliary circulating system comprised of a reservoir, a pump, and conduits.

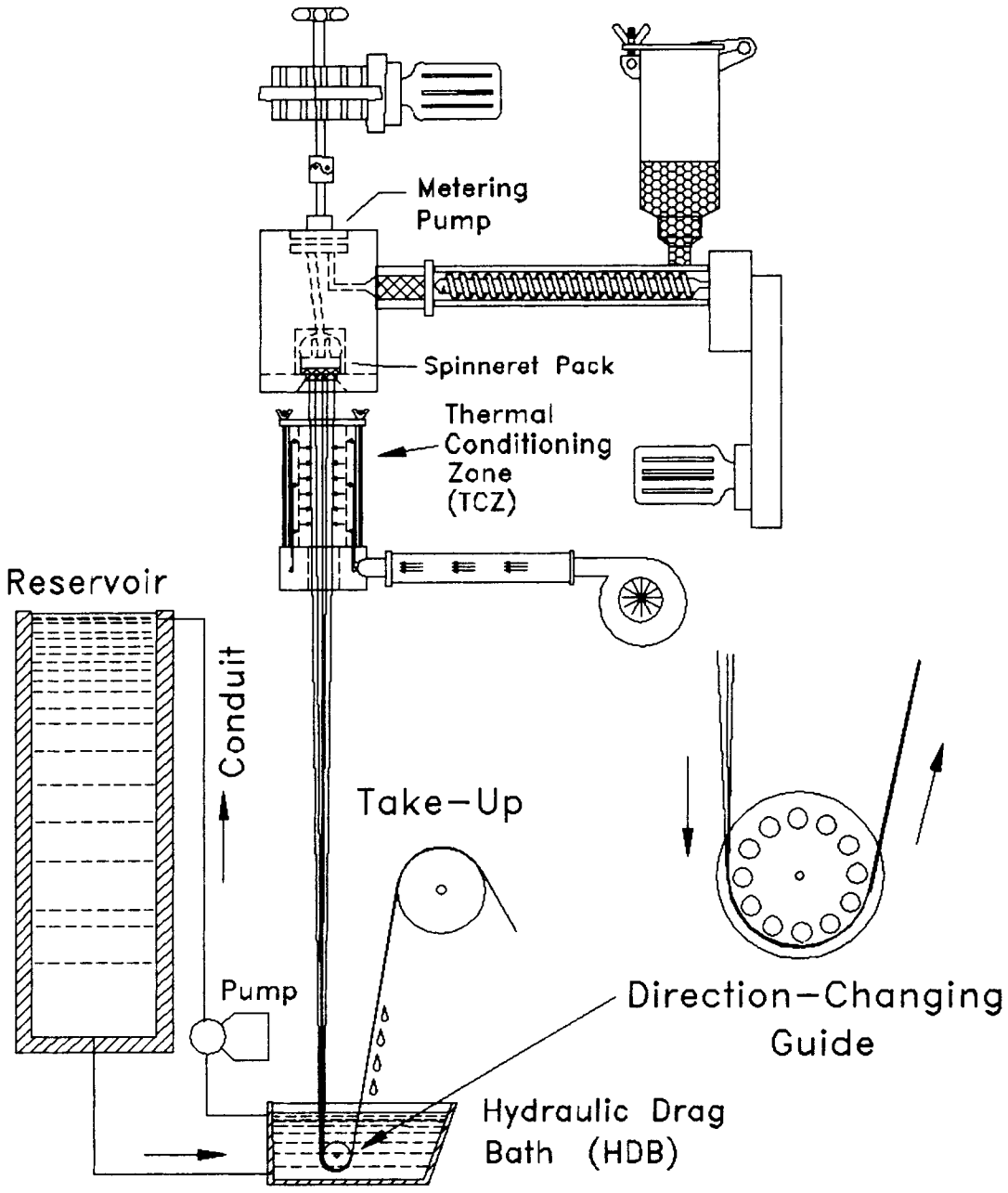

Figure 1 Melt spinning process with a thermal conditioning zone (TCZ) and a hydraulic drag bath (HDB).

In extrusion, the emerging filament from the spinneret was passed through the TCZ to delay the cooling rate in the upper region of the threadline, which was then cooled by exposure to air in the space between the TCZ and the surface of the liquid. The filament entering the HDB was directed upward to the take-up roll with a direction-changing guide, which was constructed with a set of multiple sapphire pins to reduce the angle of the snubbing drag and was located at the appropriate depth of the HDB.

Threadline Dynamics Study

Diameter Measurement

Threadline diameter was measured with a noncontact Zimmer diameter monitor (model 460 A/2) interfaced with a computer system.

Tension Measurement

Threadline tension was obtained with a Rothschild tensiometer positioned in the threadline at the point where the filament reached its final spinning speed. The tensiometer employs the usual three-point geometric path of the fiber through the unit. Therefore, the measured tension was corrected for the loss due to the centrifugal force.[12]

Force Component of Threadline

The force components along the threadline include the rheological, inertial, air drag, surface tension, and gravitational. The respective force contributions to the threadline from each component were calculated as follows:

$$F_{ext} + F_{grav} = F_{rheo} + F_{inert} + F_{drag} + F_{surf} \quad (1)$$

where

$$F_{inert} = W(V_L - V) \quad (2)$$

$$F_{surf} = \int_{R_L}^{R} \pi\sigma_s \, dR \quad (3)$$

$$F_{drag} = \int_{z}^{L} 2\sigma_d(\pi A)^{1/2} \, dz \quad (4)$$

$$F_{grav} = \int_{z}^{L} \rho A g dz \quad (5)$$

where W is the mass throughput, V_L is the take-up speed, R_L is the spun fiber radius, and A is the threadline cross section. F_{ext} is the force measured externally with a tensiometer at a position near the wind up godet. Since the force due to surface tension is insignificant, F_{surf} is neglected in the calculations. The rheological F_{rheo} can thus be obtained by the difference from Eq. (1) while the other terms are available from calculation. For the air drag term the air drag stress is calculated from

$$\sigma_d = \frac{\rho_a V^2 C_f}{2} \quad (6)$$

where ρ_a is the ambient air density. The drag coefficient C_f is based on Matsui's empirical formula[13] as shown:

$$C_f = 0.37 \, \mathrm{Re}^{-0.61} \quad (7)$$

where Re is the Reynolds number. The spinning stress is then calculated from

$$\sigma_{zz} = \frac{F_{rheo}}{A} \quad (8)$$

Temperature Profile

The temperature profile was calculated using the energy balance equation.

$$\frac{dT}{dz} = -\frac{h2\pi R(T - T_a)}{WC_p} - \frac{\sigma\epsilon 2\pi R(T^4 - T_a^4)}{WC_p} + \frac{\Delta H}{C_p}\frac{dX_c}{dz} \quad (9)$$

where h is the surface coefficient of heat transfer of the filament, C_p is the specific heat of filament, σ is the Stefan–Boltzmann constant, ϵ is the hemispherical emissivity of the fiber, ΔH is the latent heat of crystallization, and X_c is the crystallinity of the filament. In the calculation the environmental temperature T_a was measured directly with a thermocouple under various on-line heating conditions. The Nusselt number is calculated according to Kase and Matsuo,[14] using the following equation:

$$\mathrm{Nu} = \frac{2Rh}{\kappa_a} = 0.42 \, \mathrm{Re}^{0.333}\left[1 + \left(\frac{8V_y}{V}\right)^2\right]^{0.167} \quad (10)$$

where V_y is quenching air velocity and the heat conductivity of air, κ_a, is 0.808×10^{-4} cal/cm s °C. In the spinning process with a hydraulic drag bath (HDB), the heat conductivity of 0.43×10^{-3} cal/cm s °C (at 100°C) was used for 1,2-propanediol when the portion of filament was immersed in the HDB region. Radiant heat loss of the filament is assumed to be negligible since it is small compared to convective loss. The specific heat of PET is calculated according to Shimizu et al.[15] as follows:

$$C_p = 0.3 + 6.0 \times 10^{-4} \, T \quad (11)$$

According to Katayama and Yoon,[16] the heat of fusion during crystallization in the threadline, ΔH, for PET with about 40% crystallinity is 12 cal/g. In the calculations the heat generated by crystallization was assumed to be insignificant ahead of the drawing in HDB and was taken into account only beyond the drawing process in the HDB. The numerical solution of Eq. (9) was performed using the fourth-fifth order Runge–Kutta method.

Characterization of Spun Fibers

Polarizing Microscopy

A Nikon polarizing microscope equipped with a Leitz tilting compensator was used to determine the birefringence of fiber samples. The average birefringence was based on the mean value of five individual fibers.

Density Gradient Column

Fiber density was measured at 23°C using a density gradient column filled with sodium bromide solution in the density range of 1.335–1.415 g/cm^3. The sample preparation and density measurement were in accordance with ASTM standard D1505-68. The weight fraction crystallinity was calculated from the density method by applying the equation:

$$X_c = \frac{(\rho - \rho_a^\circ)\rho_c^\circ}{(\rho_c^\circ - \rho_a^\circ)\rho} \tag{12}$$

and the volume fraction crystallinity was calculated from the equation:

$$X_c = \frac{\rho - \rho_a^\circ}{\rho_c^\circ - \rho_a^\circ} \tag{13}$$

where ρ is the density of the fiber, ρ_c° is the density of the crystalline phase, and ρ_a° is the density of the amorphous phase. The values of ρ_c° and ρ_a° used in the calculation for PET are 1.455 and 1.335 g/cm^3, respectively.[17]

Wide-Angle X-Ray Scattering (WAXS)

A Siemens type-F X-ray diffractometer system equipped with a nickel-filtered CuK_α (λ = 1.5418 Å) radiation source and a proportional counter was used in the analysis of the crystalline structure of PET samples. The sample was prepared as a bundle of parallel fibers. For a crystalline high-speed spun PET fiber sample, the equatorial diffraction presents three distinct reflections, (010) at 2θ = 18°, (;$\bar{1}$10) at 2θ = 23°, and (100) at 2θ = 26°. The profile of the equatorial diffraction was first corrected for the amorphous scattering with the scan in the meridional direction. Then, the equatorial diffraction profile was resolved using the Pearson VII formula as discussed by Heuvel and Huisman.[18]

$$f(x) = \frac{I_{0i}}{\left[1 + 4\left(\frac{x - x_{0i}}{\beta}\right)^2 (2^{1/m} - 1)\right]^m} \tag{14}$$

where I_{0i} is the peak height, x_{0i} is position of the center of the peak, β is halfwidth, and m is a shape parameter.

The apparent crystallite size was determined according to the Scherrer equation:[19]

$$L_{hkl} = \frac{K\lambda}{\beta \cos\theta} \tag{15}$$

where β is the half width of the diffraction peak, K is taken to be unity, θ is the Bragg angle, and λ is the wavelength of X-ray used. The interplanar spacing d was calculated from the Bragg equation:

$$n\lambda = 2d \sin\theta \tag{16}$$

where n is the constant 1 (first order). The crystalline orientation factor, f_c, is related to $\langle \cos^2\phi_{c,z} \rangle$ as follows:

$$f_c = \tfrac{1}{2}\left(3\langle \cos^2\phi_{c,z} \rangle - 1\right) \tag{17}$$

where $\phi_{c,z}$ is the angle between the c crystallographic axis and the fiber axis. In PET there is no meridional plane to give measurable diffraction. The only plane that is likely to give appreciable intensity and that lies near the meridian is the ($\bar{1}$05) plane. There is a small amount of azimuthal overlapping between the ($\bar{1}$05) and (0$\bar{2}$4) planes. The overlapping can be resolved using the Pearson VII model as stated previously. Since the amorphous diffraction is small above 2θ = 36° while the ($\bar{1}$05) peak occurs at 2θ = 43°, correction for amorphous scattering is unnecessary. The value of $\langle \cos^2\phi_{c,z} \rangle$ is determined from azimuthal intensity measurements on the reflection of ($\bar{1}$05) with the following equations:[20]

$$\langle \cos^2\phi_{\bar{1}05,z} \rangle = \frac{\int_0^{\pi/2} I(\phi)\sin\phi\cos^2\phi\, d\phi}{\int_0^{\pi/2} I(\phi)\sin\phi\, d\phi} \tag{18}$$

$$\langle \cos^2\phi_{c,z} \rangle = \frac{\langle \cos^2\phi_{\bar{1}05,z} \rangle}{\cos^2\alpha} \tag{19}$$

where $\phi_{\bar{1}05,z}$ is the angle between ($\bar{1}$05) reflection plane normal and the fiber axis and α is the angle

between ($\bar{1}05$) reflection plane normal and the c crystallographic axis.

The amorphous orientation factor, f_a, was determined using the following relationship:

$$\Delta n = \Delta n_c^\circ f_c X_c + \Delta n_a^\circ f_a (1 - X_c) \qquad (20)$$

where Δn is the total birefringence of fiber measured by polarizing microscopy, X_c is the volume fraction crystallinity from the density method, and Δn_c° and Δn_a° are the respective intrinsic birefringences of the crystalline and the amorphous regions. The values of Δn_c° and Δn_a° are 0.22 and 0.275.[21]

Small-Angle X-Ray Scattering (SAXS)

An evacuated small-angle camera of moderately high resolution originally designed by W. O. Statton was used for the photographic X-ray diffraction analysis. A fiber sample holder with a pinhole collimator of 0.25 mm diameter and a sample-to-film distance of 32 cm were used. The long period spacing (LPS) was calculated from a measurement of the separation of quadrant spots or meridional streaks in a direction parallel to the fiber axis by application of the Polanyi equation.[22]

$$n\lambda = \ell \sin \Phi \qquad (21)$$

where n is the constant unity for first-order layer lines, ℓ is the long period spacing of repeat lamellar structure, and Φ is half the angular separation of the quadrant spots or streaks measured parallel to the fiber axis. The long period spacing ℓ can be expressed with the sample to film distance, $\mathcal{F}$, and the spots or streaks separation, $\mathcal{L}$, using the approximation of $\Phi = \sin \Phi = \tan \Phi$ at small angle:

$$\ell = \frac{\lambda}{\sin \Phi} = \frac{\lambda}{\tan \Phi} = \frac{2\lambda\mathcal{F}}{\mathcal{L}} \qquad (22)$$

Interference Microscopy

Radial distribution of structure was determined with a Jena interference microscope interfaced to a computer imaging system developed in our laboratory.[23] The radial birefringence and Lorentz density were calculated, in turn, from the local refractive indices ($n_{\|}$ and $n_{\perp}$) parallel and perpendicular, respectively, to the fiber axis by the shell model assumption.

Differential Scanning Calorimetry (DSC)

A Perkin-Elmer Series 7 thermal analysis differential scanning calorimeter was used to obtain thermal traces of the fibers. DSC curves were obtained during the first heating of ca. 8 mg fiber sample at a heating rate of 10 K/min.

Boil-Off Shrinkage (BOS)

Boil-off shrinkage was determined by loading a parallel bundle of unconstrained fibers in boiling water for 5 min in accordance with ASTM D2102-79. The percent shrinkage was calculated as

$$\text{BOS} = \left(1 - \frac{l}{l_0}\right) \times 100 \qquad (23)$$

where l_0 is the initial length and l is the final length of the fibers.

Instron Tensile Tester

A table model 1122 Instron tensile tester was used to measure tenacity, ultimate elongation, and initial modulus in accordance with ASTM D3822-82. The fiber sample was tested at a gauge length of 25.4 mm and at a constant crosshead speed of 20 mm/min. An average of at least five individual tensile determinations was obtained for each sample.

RESULTS AND DISCUSSION

Threadline Attenuation, Cooling, and Stress Profiles

Typical diameter and velocity profiles for the threadline of PET melt spinning with TCZ (250°C) and HDB (110°C and 28-cm path length) are shown, respectively, in Figures 2 and 3. Additionally, profiles from the high-speed spinning, 3000 and 6500 m/min, with TCZ only are included in the figure for comparison, as indicated by dashed lines. With the HDB present, the attenuation processes of all three different take-up speeds tested are nearly undistinguishable. The only differences that can be seen are in the velocity profiles, especially in the region beyond the HDB. The diameter profiles in the upper portion of the threadline are smooth and similar to those of the normal high-speed spinning process. The diameters are gradually reduced down to a point 65 cm from the spinneret, after which the diameters remain constant until the fiber enters the HDB. In this process the filament shows a rapid attenuation in the region of HDB. Since no diameter data were collected in the liquid bath, the diameter profiles within the HDB were attained by interpolation of

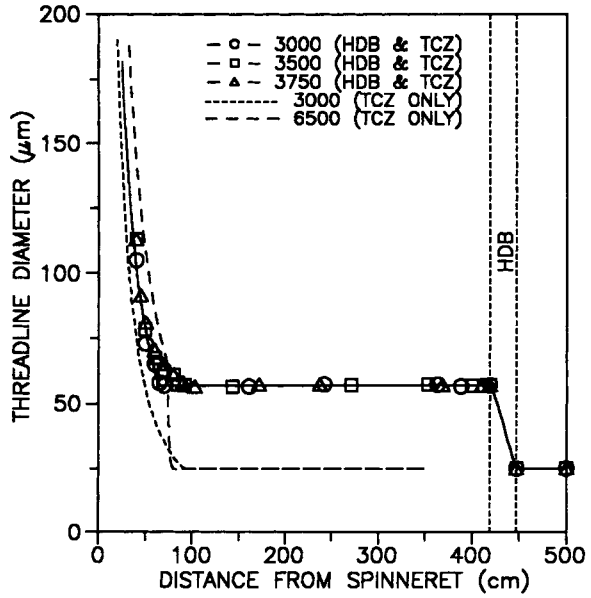

Figure 2 The effect of HDB on the diameter profile of PET (IV = 0.95) threadline spun at various take-up speeds.

data measured before and after the HDB. However, it is believed that the attenuation is in a more abrupt manner, very similar to the necklike deformation in the case of high-speed spinning. In Figure 2, when it is compared with the diameter profile of the high-speed spinning process at 3000 m/min with the use of TCZ only, indicated with dashed line, the attenuations in the upper portion of the spinning process with HDB are delayed and the filament diameters are larger. And then the draw-down ratios within the HDB are similar, a value of ca. 5.2, for all three different testing take-up speeds. It is speculated that different properties of the HDB spun fibers with different take-up speeds might greatly attribute to the different stress levels induced by the take-up speeds rather than the draw-down ratio of threadlines in the HDB.

Figures 4 and 5 show, respectively, the diameter and velocity profiles of the HDB spinning process at different spinning deniers. Similar to Figures 2 and 3, a two-stage draw-down occurs in this experiment. The different attenuation rates in the upper portion of threadlines of different spinning deniers are the effect of mass throughput and cooling rate; the increase of mass throughput causes the reduction of cooling rate, and hence the slower attenuation process. From the calculation of draw-down ratio within the HDB, threadline of 7.0 dpf (denier per filament) has slightly higher draw-down ratio than that of 5.0 dpf, with the values of 5.36 versus 5.2. However, from the properties of final spun fibers, as discussed in later sections, the increase of spinning denier yields a reduction of the molecular orientation. The results further support that the spinning stress rather than the draw-down ratio is the

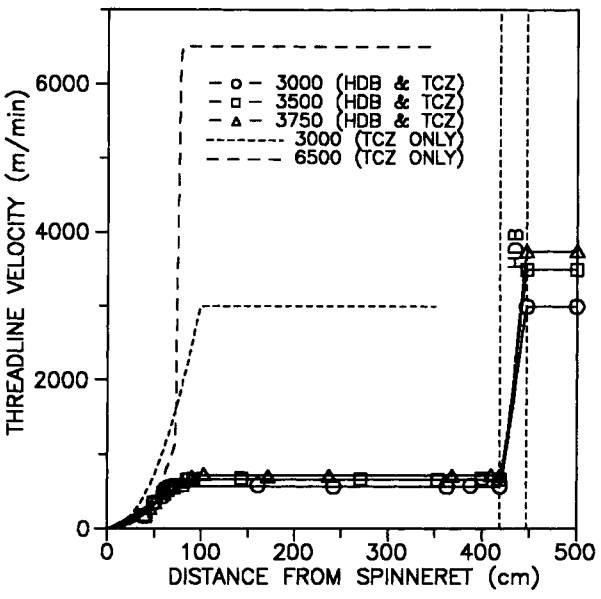

Figure 3 The effect of HDB on the velocity profile of PET (IV = 0.95) threadline spun at various take-up speeds.

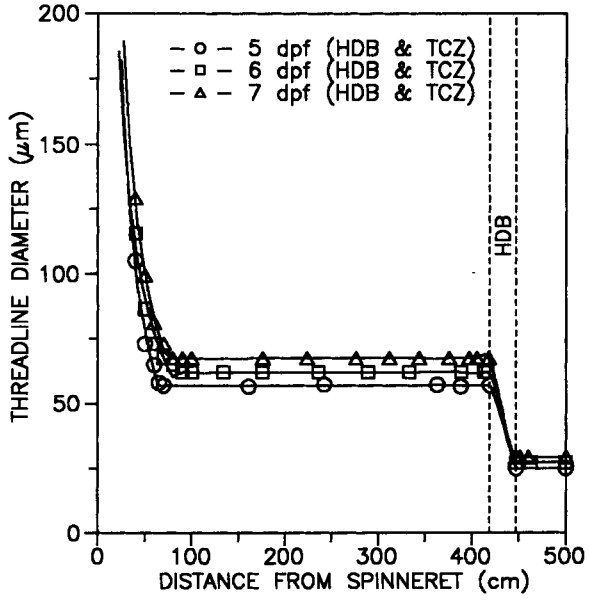

Figure 4 The effect of spinning denier on the diameter profile of PET (IV = 0.95) threadline spun at 3000 m/min with TCZ (250°C) and HDB (110°C and 28 cm).

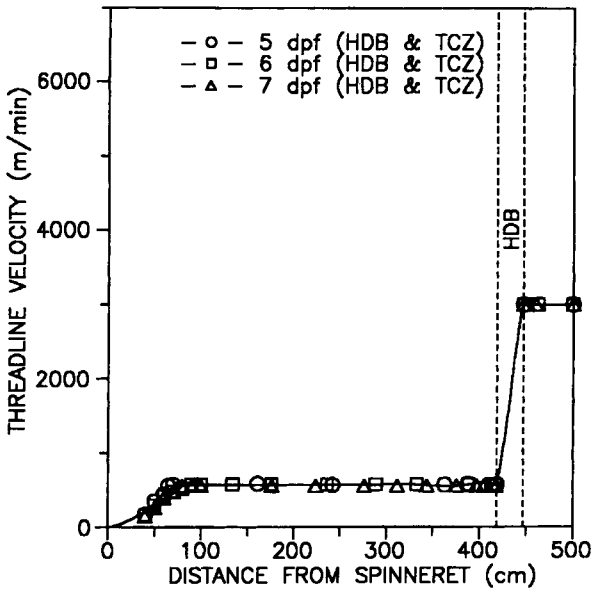

Figure 5 The effect of spinning denier on the velocity profile of PET (IV = 0.95) threadline spun at 3000 m/min with TCZ (250°C) and HDB (110°C and 28 cm).

main factor affecting the molecular orientation developed in the spinning process using the HDB.

Figure 6 shows the temperature variation along the threadline of the spinning process using the HDB (110°C and 28 cm path length) at various take-up speeds. At a constant spinning denier, the effect of take-up speed on the temperature profile is small. The filament reaches ambient temperature at ca. 250 cm from the face of spinneret. In the HDB the filament is heated rapidly by the liquid medium to approximately the temperature of the bath, 110°C.

In this region the filament temperature is higher than the glass transition temperature of PET, T_g = 70°C. Therefore, the structure can be developed coincidently with increase of the thermal mobility of the molecular chains while the filament is elongated rapidly under a high level of stress. In normal high-speed spinning the spinning stress at the end of a necklike deformation is very important in determining the extent of molecular orientation developed. The spinning stress is strongly related to the inertial and air drag forces contribution in the region of the neck. The spinning process with the HDB provides another degree of freedom for control of the stress in the region of the structure development. Comparing the spinning process as shown in Figure 7, the spinning stress can be increased substantially with the HDB in place. The spinning stress at the exit of the HDB (110°C and 28 cm path length) is 3.14 gf/d at 3000 m/min take-up speed compared with the spinning stress of 0.11 gf/d at the end of neck of a high-speed spinning process at 6000 m/min using only TCZ. This represents about a 28.5 times increase. The air drag contribution from

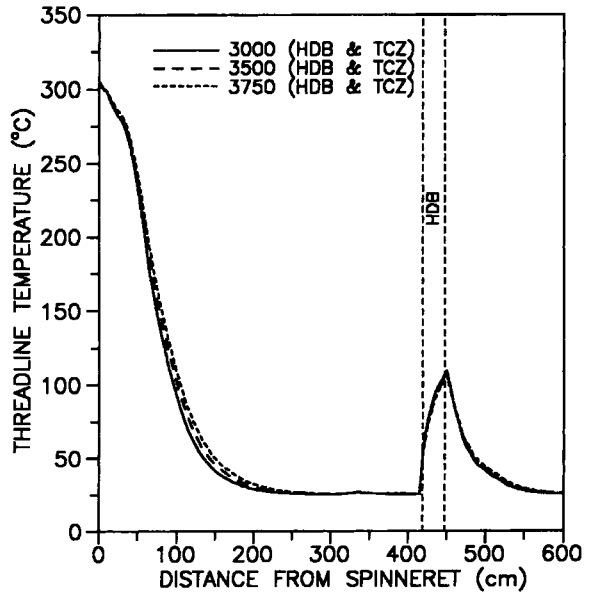

Figure 6 The effect of HDB (110°C and 28 cm) on the temperature profile of PET (IV = 0.95) threadline spun at various take-up speeds.

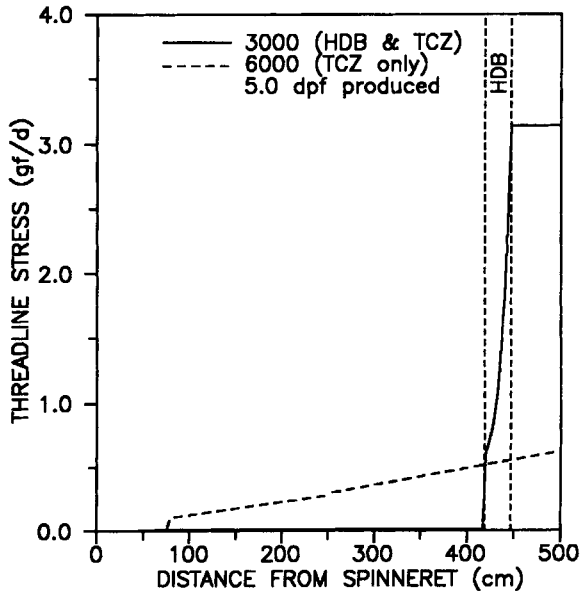

Figure 7 Comparison of stress profiles of PET (IV = 0.95) threadline spun at 3000 m/min (TCZ and HDB) and at 6000 m/min (TCZ only).

the entire threadline is only a small fraction of the spinning stress in the case of the HDB spinning process. The high spinning stress is governed mainly by the drag force from the liquid medium.

The amount of the increase of the spinning stress with the HDB in place depends greatly on several parameters, namely the take-up speed, the HDB path length, the spinning denier, and the HDB temperature. Figure 8 shows the effect of take-up speed on the stress at the exit of HDB. Due to the high level of tension in the threadline after passing the HDB, in which the force measured for a 5-dpf threadline at 3000 m/min take-up speed can reach 18.5*g*, force measurements at higher take-up speed or lower spinning denier became impossible due to the excessive breakage when the tensiometer is placed in the threadline. The spinning stress of the threadline before entering the HDB remains the same regardless of the increase of take-up speed. This explains how the major structure development is completed in the HDB, in which the stress and temperature are controlled under favorable conditions.

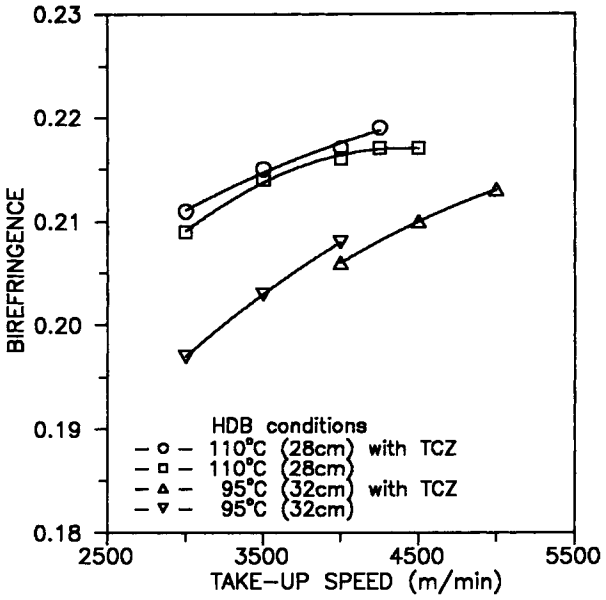

Figure 9 Birefringence vs. take-up speed for PET (IV = 0.95) fibers pun with and without TCZ at different HDB conditions.

Properties of Spun Fibers

Birefringence of PET fibers spun in the speed range of 3000–5000 m/min at HDB conditions is shown in Figure 9. It is surprising that a high birefringence value is obtained at 3000 m/min take-up speed with the water temperature in the HDB at only 95°C. At 3000 m/min take-up speed, the birefringence with the HDB path length at 32 cm is more than three times greater than that of the ordinary high-speed

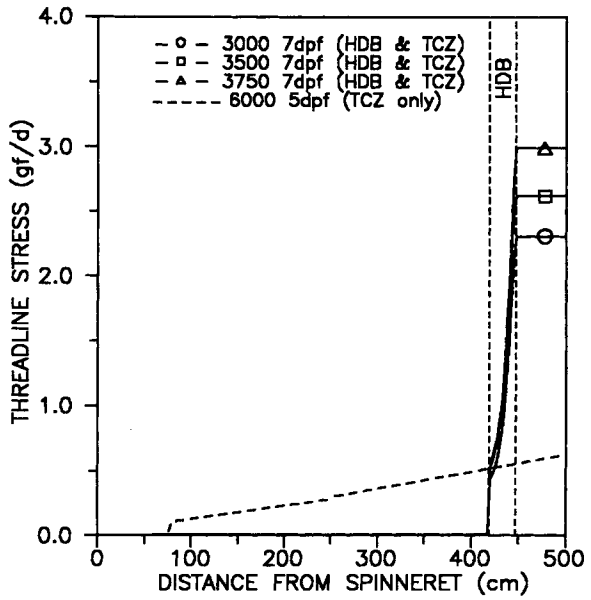

Figure 8 The effect of take-up speed on the stress profiles of PET (IV = 0.95) threadline spun with TCZ (250°C) and HDB (110°C and 28 cm).

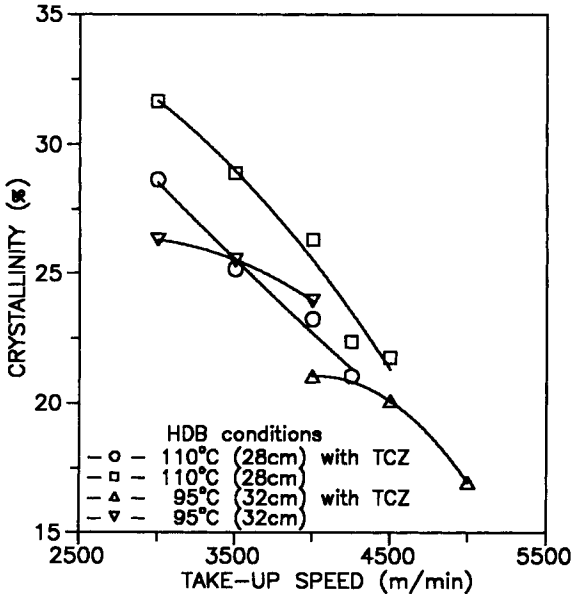

Figure 10 Crystallinity vs. take-up speed for PET (IV = 0.95) fibers pun with and without TCZ at different HDB conditions.

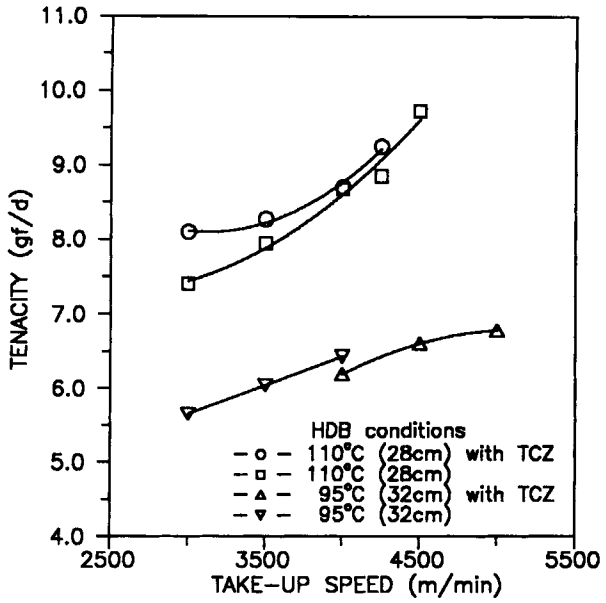

Figure 11 Tenacity vs. take-up speed for PET (IV = 0.95) fibers spun with and without TCZ at different HDB conditions.

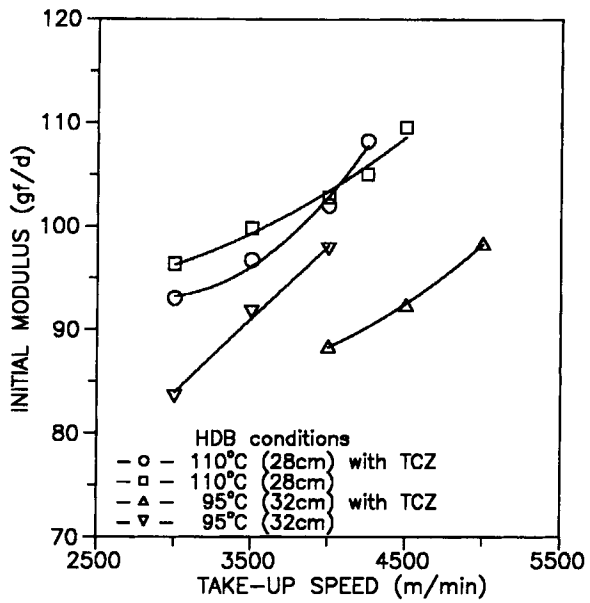

Figure 13 Initial modulus vs. take-up speed for PET (IV = 0.95) fibers spun with and without TCZ at different HDB conditions.

spun fiber, which is ca. 0.05. With the increasing take-up speeds, the birefringence of fibers spun with HDB of 110°C and 28 cm reaches an asymptotic region at 4250 m/min take-up speed. The birefringence of fibers thus obtained is 0.217, a value quite close to the intrinsic crystalline birefringence value, 0.22, as reported by Dumbleton.[21] The level off of birefringence suggests that probably a saturated level of molecular orientation has been reached. In addition to the use of the HDB, the TCZ was also

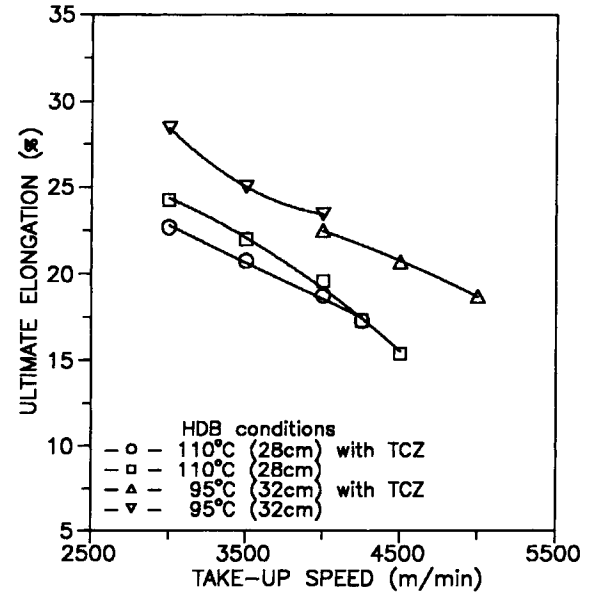

Figure 12 Ultimate elongation vs. take-up speed for PET (IV = 0.95) fibers spun with and without TCZ at different HDB conditions.

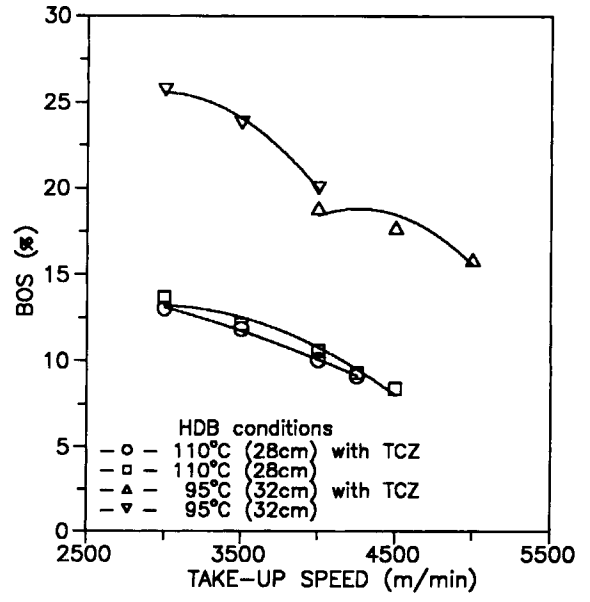

Figure 14 Boil-off shrinkage vs. take-up speed for PET (IV = 0.95) fibers spun with and without TCZ at different HDB conditions.

Table I Typical Properties of HDB Spun Fibers before and after Drawing and Annealing

Fiber	Birefringence	Tenacity (gf/d)	Initial Modulus (gf/d)	Ultimate Elongation (%)	Crystallinity (%)
HDB-Spun[a]	0.221	8.2	113	15.7	24.8
Drawn and Annealed[b]	0.237	10.2	114	10.0	48.5

[a] Spinning condition: Polymer: 0.95 IV PET; spinning speed: 3500 m/min; spun fiber denier: 5 dpf; TCZ: 250°C; HDB temperature: 110°C; HDB path: 28 cm.
[b] Drawing and annealing condition: Preheat roll: 90°C; hot plate: 250°C, 10 in.; draw ratio: 1.2; take-up speed: 10 m/min.

utilized to further enhance the properties. The further increase of birefringence of fibers spun with HDB of 95°C and 32 cm path length as a function of take-up speed above 4000 m/min was mainly due to the improvement of spinning stability when TCZ was applied. When the HDB was set at 110°C and 28 cm path length, the addition of TCZ shows insignificant improvement of spinning stability, but it shows a measurable amount of improvement in birefringence. It is speculated that TCZ may help increase the molecular orientation in the filament as a structure formation precursor before proceeding to the rapid structure developing zone in the HDB.

Another effect of using higher temperature in the HDB is readily seen from the higher crystallinity of spun fibers as shown in Figure 10. The difference in crystallinity, compared to the process with HDB of 95°C, is more significant at lower take-up speed than at higher take-up speed. It is noted that the crystallinity is a decreasing function of take-up speed irrespective of the use of a higher HDB temperature.

Likewise, the increase of T/E/M as a function of take-up speed, as shown in Figures 11, 12 and 13, is in accordance with the increase of birefringence, showing that high level of molecular orientation leads to the substantial improvement of T/E/M values. The lack of data at higher take-up speeds or at longer HDB path length was due to frequent breakage occurring in the threadline. The breakage was likely attributed to the insufficient time for the molecular chains to rearrange to comply with the rapid deformation at the high level of stress. It needs to be pointed out that at 4500 m/min take-up speed, the tenacity of fibers spun with the HDB at 110°C is 9.72 gf/d, a value exceeding the tenacity of fibers from the current industrial two-step spin-draw process; low-speed spun and mechanically drawn.

In spite of the high level of molecular orientation, the crystallinity of fibers spun with the HDB process still presents a decreasing function of take-up speed. First, it might be speculated that possible microvoids are formed in the spun fibers under high level of stress as is the case of ordinary high-speed spinning,[24,25] which tend to decrease the density of the fiber. Interference microscopy and wide angle X-ray diffraction studies, to be discussed later, prove that the decrease of density as well as that of crystallinity is a real feature rather than an artifact arising from the formation of microvoids. The formation of a highly oriented structure, as shown in the high level of birefringence, accompanied by a distinct lower level of crystallinity leads to another speculation, namely, that a high fraction of an intermediate state of order, termed mesophase, may exist between the

Table II Properties of HDB Spun Fibers Spun under Different Spinning Speeds and HDB Temperatures[a]

Spinning Speed (m/min)[b]	HDB Temperature (°C)	Tenacity (gf/d)	Ultimate Elongation (%)	Initial Modulus (gf/d)	Birefringence	Crystallinity (%)	Boil-off Shrinkage (%)
4750	120	7.5	25.9	112	0.217	27.3	15.5
4500	150	6.8	22.6	109	0.194	36.4	6.4
4250	180	6.8	26.6	103	0.189	43.1	5.9

[a] Spinning condition: Polymer: 0.95 IV PET; TCZ: 250°C; HDB path: 12 cm.
[b] Maximum attainable spinning speed.

Table III Properties of HDB and TCZ Spun Fibers at Different Spinning Denier

Spinning Denier (dfp)	Tenacity (gf/d)	Ultimate Elongation (%)	Initial Modulus (gf/d)	Birefringence	Crystallinity (%)	Boil-off Shrinkage (%)
4.5	11.8	21.5	126	0.220	22.3	10.9
5.0	8.7	18.8	102	0.216	23.3	10.1
6.0	8.0	16.9	97	0.204	26.7	12.8
7.0	7.6	24.8	92	0.209	27.9	13.8

[a] Spinning condition: Polymer: 0.95 IV PET; spinning speed: 4000 m/min; TCZ: 250°C; HDB temperature: 110°C; HDB path: 28 cm.

amorphous and the crystalline phase in the HDB spun fibers. This was also supported by results from the boil-off shrinkage (BOS) test. In Figure 14 the BOS shows a decreasing, rather than increasing, function of the take-up speed; the crystallinity also decreases with the increase of take-up speed. This result is different from the ordinary high-speed spinning and strongly supports the existence of mesophase since the thermal relaxation of molecular chains in the mesophase requires a higher temperature than the boiling point of water. The existence of a mesophase in PET was first reported by Jellinek et al.[26] in their study of PET fibers subjected to thermal treatment at different temperatures and stresses. More recently, Shimizu et al.[27] reported that the oriented molecular chains in the mesophase can readily aggregate and then initiate the nucleation of crystals. This was proved in a further drawing and annealing step of the HDB spun fibers as shown in Table I. Upon drawing and annealing of the HDB spun fiber, the fiber crystallizes further to the very high level of 48.5%.

The mechanism of the formation of fibers consisting of a very rich mesophase structure rather than the crystalline structure is still unclear. Even though two driving forces, stress and supercooling, are favorable for the crystallization to proceed in the HDB spinning process, it is speculated that the extremely high level of stress during the structure development period hamper the rotational freedom of C–C and C–O bonds between the aromatic rings. In order for crystallization to proceed, a certain degree of rotational freedom of C–C and C–O bonds is necessary for the rearrangement of ethylene glycol units aligned in the all-*trans* conformation. George[28] indicated that under the large driving forces of supercooling and stress, the critical size for a stable nucleus approaches the dimensions of the crystal unit cell. Under this condition the mechanism of crystallization changes from a nucleation growth to a rather rapidly homogeneous phase transformation. Therefore, fine-grained crystallites could be formed with many extended tie molecules connecting the crystallites leaving none or few chain folds at the boundary of crystalline region.

With the increase of HDB temperature, a notable decrease of spinning stability was readily observed. The decrease of the maximum attainable spinning speed with the increase of the HDB temperature, as shown in Table II, is speculated to be a consequence of the rapid deformation of the filament in the HDB.

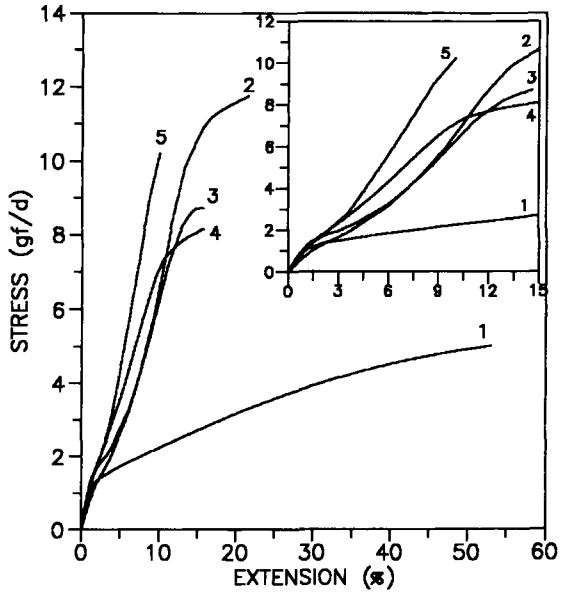

Figure 15 Typical stress–strain curves for PET (IV = 0.95) fibers under different spinning and posttreatment conditions: (1) 5 dpf spun at 6000 m/min with TCZ (250°C); (2) 4.5 dpf spun at 4000 m/min with TCZ (250°C) and HDB (110°C and 28 cm); (3) 4 dpf commercial spun-drawn tire cord yarn; (4) 5 dpf spun at 3500 m/min with TCZ (250°C) and HDB (110°C and 28 cm); (5) drawing (1.2/1) and annealing (250°C) of sample 4.

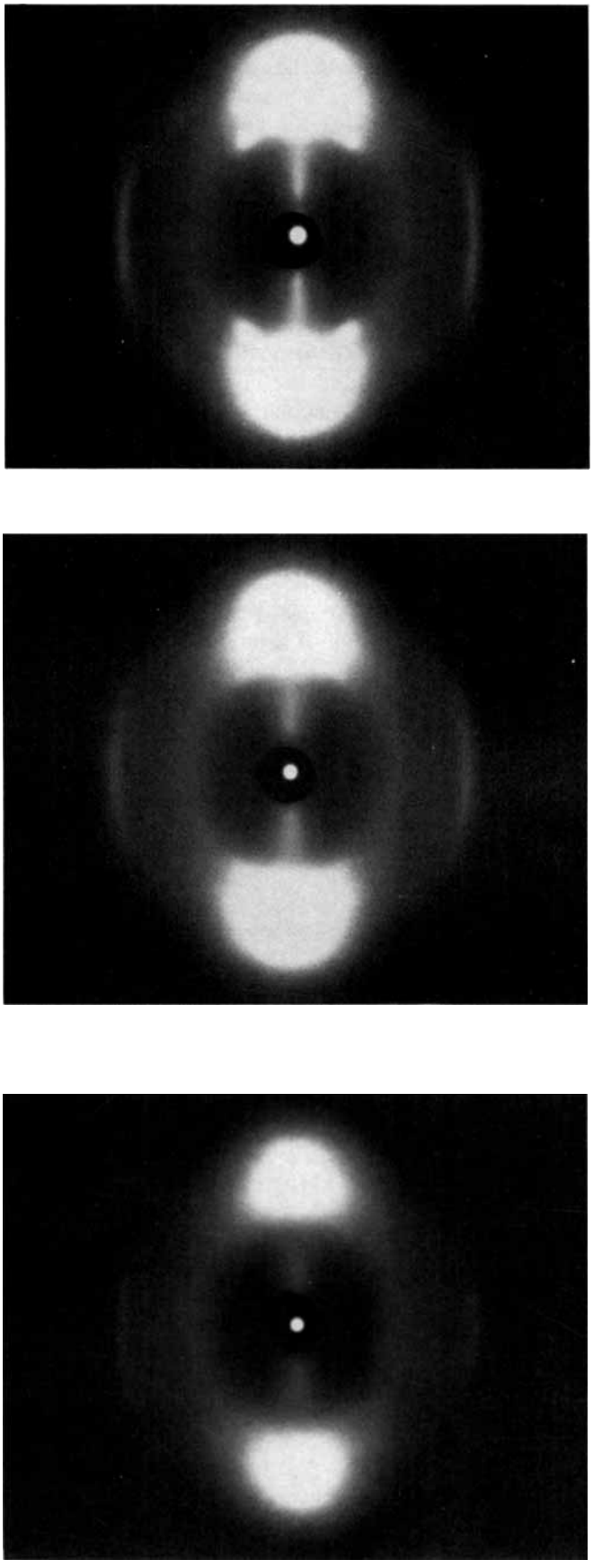

Figure 16 WAXS patterns of PET filaments obtained at various conditions: (a) 5500 m/min take-up with HDB (25°C and 8 cm); (b) 5500 m/min take-up with TCZ (250°C) and HDB (95°C and 32 cm); (c) 4000 m/min take-up with TCZ (250°C) and HDB (110°C and 28 cm).

At high HDB temperature with a small increase of the take-up speed, the deformation rate of threadline in the HDB can increase exponentially. Therefore, under this extreme spinning condition, the spun fiber properties as well as the spinning stability are a sensitive function of HDB temperature. At 180°C HDB temperature, a temperature near the boiling point of 1,2-propanediol, the fibers thus spun possess a high degree of crystallinity, 43.1%, a level comparable to the traditional high-speed spun fibers. The lower BOS of fibers produced through the higher HDB temperature is mainly due to the increase of crystallinity.

Table III shows properties of fibers spun with HDB at different spun fiber deniers. The take-up speed was set at 4000 m/min, and therefore the spun denier was controlled by adjusting the mass throughput. In ordinary high-speed spinning, the spinning denier has little or almost no effect on the spun fiber properties, and the properties are mainly controlled by the take-up speed. However, the results in Table III show that the spun fiber properties are greatly affected by the change of denier. Very high tenacity and initial modulus, 11.8 and 126 gf/d, were obtained at 4.5 dpf spinning process with HDB. At these spinning conditions, the decrease of spinning denier below 5.0 dpf has a profound effect on the tenacity and initial modulus of fibers. In this experiment slightly further decrease of spinning denier below 4.5 dpf starts to cause a high frequency of breakage in the threadline. Intuitively, this can be understood as the decrease of spinning denier, as well as the decrease of cross-sectional area of filament, which means an increase of stress under constant threadline force.

In spite of the high level of tenacity and initial modulus, the ultimate elongation of the fibers is still high, which is not improved by a decrease of the spinning denier. The dependence of crystallinity on the spinning denier is also obvious. The fibers spun at greater spinning denier can crystallize better than those of finer denier. In other words lower stress with greater spinning denier can improve the crystallization process in the threadline. This result further supports the previous interpretation of the hindrance of crystal growth under extremely high levels of stress.

Figure 15 shows comparison of stress–strain curves for PET fibers produced with different techniques. The denoted numbers represent different spinning or posttreatment conditions, which are included in the description of Figure 15. Curves 2 and 4 are the typical stress–strain curves of HDB spun fibers. Unlike the fiber spun with high-speed spinning, denoted as curve 1, the HDB spun fibers exhibit an obvious deflection in the yielding region, and the strength increases drastically with the elongation after being strained beyond the yielding length. Thereafter, the strength reaches a plateau region before the breakage occurs as the elongation further increases. The plateau region of HDB spun fibers is very significant compared with that of the spun–drawn fiber. Upon the further drawing and annealing steps of sample 4, the posttreated fibers, denoted as 5, show that the strength increases monotonically with the strain. The yield deflection of the posttreated HDB spun fibers is not obvious, and the upper plateau region before the breakage disappears. This phenomenon might be related to the fact that the posttreated HDB spun fibers have a high degree of molecular orientation and crystallinity.

Structure of Spun Fibers

Typical WAXS patterns of PET fibers spun at various conditions with the HDB are shown in Figure 16. Despite the high birefringence of the fibers produced, the patterns show an unresolved, diffuse diffraction concentrated toward the equator, indicating oriented molecules in the small crystallites and predominantly amorphous samples. In high-speed spinning at 5000 m/min, for example, a well-resolved diffraction of the WAXS pattern normally

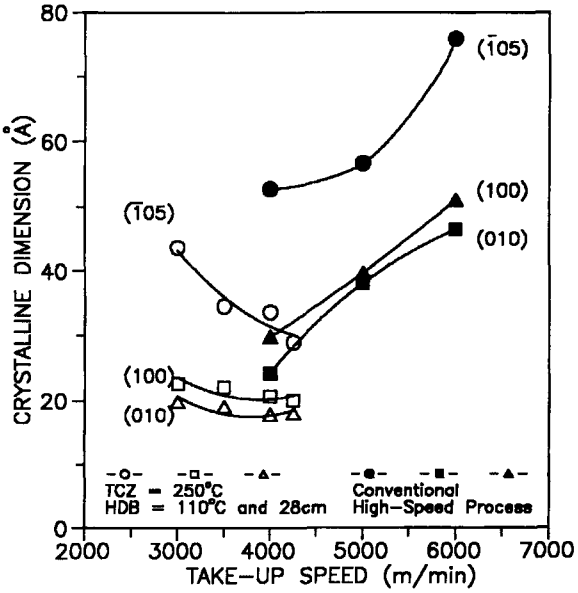

Figure 17 Crystalline dimension vs. take-up speed for PET (IV = 0.95) fibers spun with TCZ (250°C) and HDB (110°C and 28 cm).

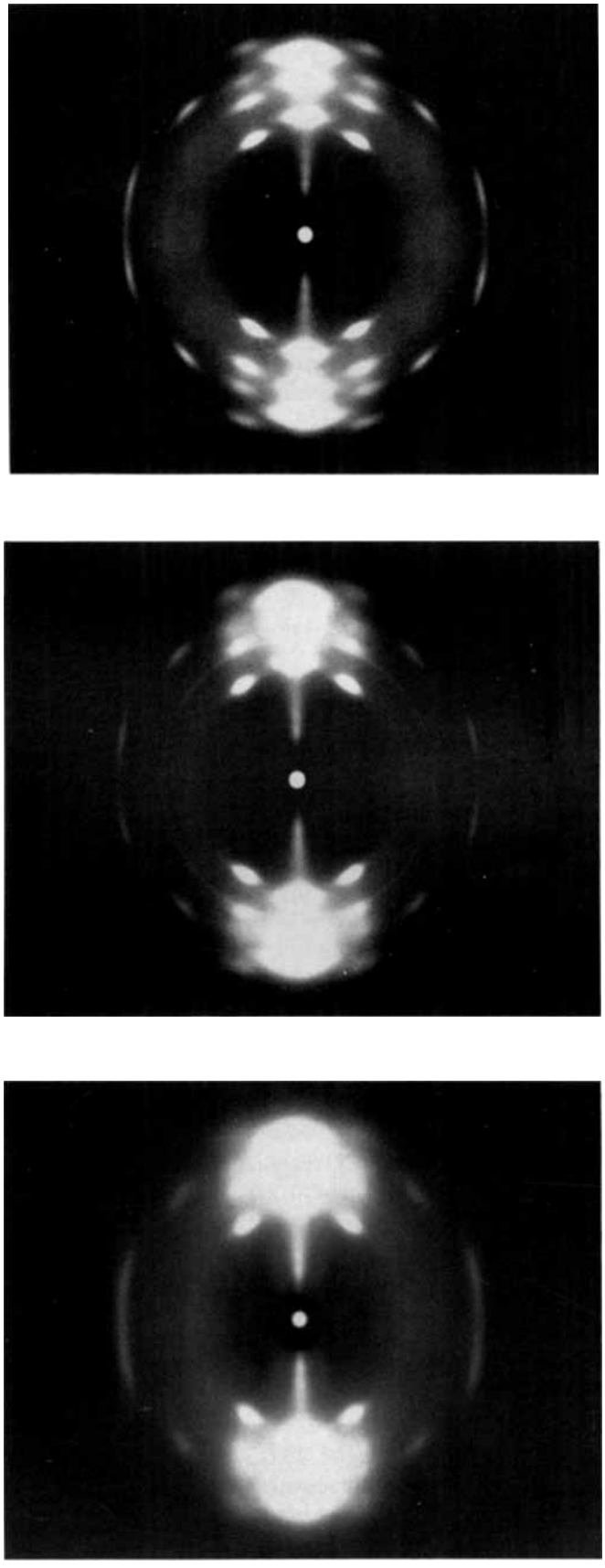

(a) (b) (c)

Figure 18 WAXS patterns of PET filaments obtained under various conditions: (a) 3250 m/min take-up with HDB (150°C and 28 cm); (b) 4250 m/min take-up with HDB (180°C and 12 cm); (c) 6000 m/min take-up with TCZ (250°C).

can be seen in the equatorial direction. Lack of this characteristic in the HDB process indicates that the great crystallite sizes found in the fibers spun with the ordinary high-speed spinning process are suppressed when the HDB is introduced into the spinning process. With increase of the HDB temperature from 25 to 95°C and further to 110°C, shown in sequence of Figure 16(a), (b), and (c), the gradual emergence of the meridional arc of the ($\bar{1}05$) reflection plane indicates the occurrence of increasing crystalline orientation. Crystallite dimensions in the direction of each of the reflection planes were calculated from the half width of diffraction peaks, (010), (100), and ($\bar{1}05$). Dependence of crystalline dimension on the take-up speed of the HDB spinning process is shown in Figure 17. With an increase in the take-up speed, the crystalline dimension in the directions of the (010) and the (100) reflection planes, which is in the transverse direction to the axis of an oriented fiber, is reduced slightly while the dimension in the direction of the ($\bar{1}05$) reflection, the fiber direction, decreases rapidly. It may be reasoned that the suppression of the crystallite size occurs mainly in the fiber direction under high take-up speed corresponding to the accompanying high spinning stress.

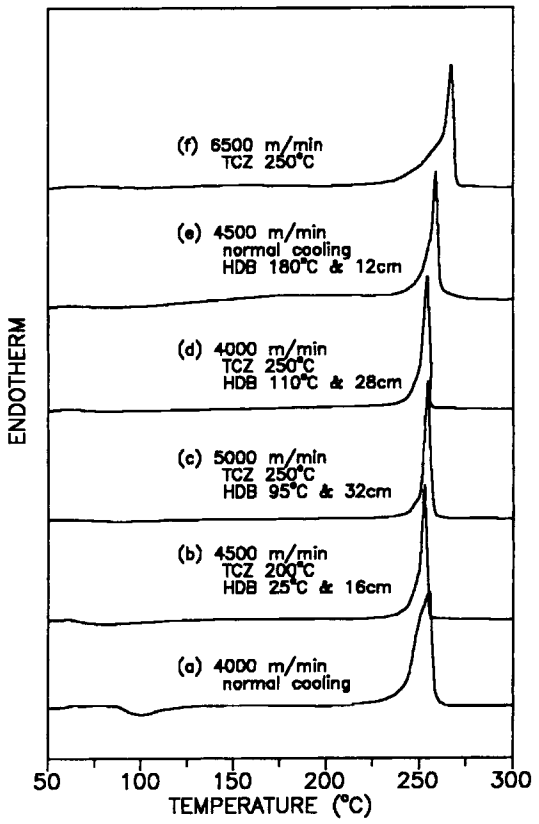

Figure 19 DSC curves of PET (IV = 0.95) fibers spun under various conditions.

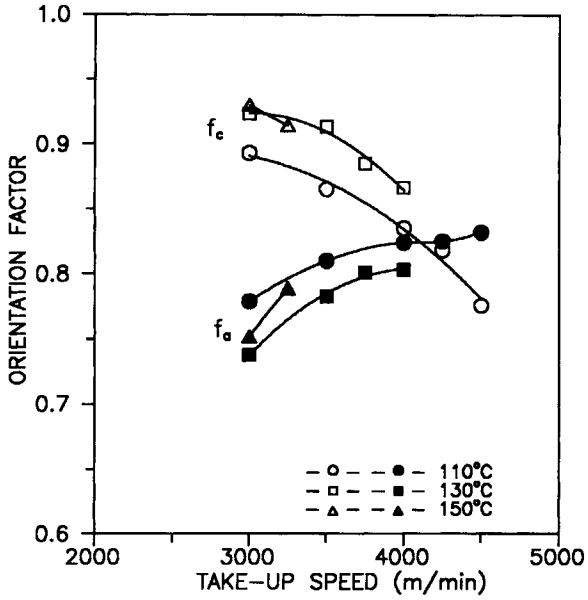

Figure 20 Crystalline (f_c) and amorphous (f_a) orientation factors for PET (IV = 0.95) fibers spun at different HDB temperatures.

Distinct WAXS patterns can be seen with the increase of HDB temperature as shown in Figure 18(a) and (b). An increase in the HDB temperature may promote crystal growth possibly by virtue of the increase of local molecular mobility, which compensates for the constraint of the molecular chains induced by the high spinning stress. It must be pointed out that the WAXS patterns of fibers spun with the HDB at 180°C resemble the patterns of fibers spun at high take-up speed with TCZ (250°C).

DSC diagrams of fibers spun under different spinning conditions are given in Figure 19. As shown in the curve (a), fibers spun at 4000 m/min exhibit a crystallization exotherm with a peak temperature near 100°C and then a melting endotherm at 255.4°C. The exotherm crystallization peak is related to thermally induced crystallization during the heating process of the DSC scan. In other words the fiber sample is not highly crystallized during the spinning process and can further crystallize under the heating process of the DSC. In fact, sample (a) has only 28% crystallinity. At 6500 m/min take-up speed, the spun fibers crystallize to a very high extent, 42.6%, and the exotherm crystallization peak disappears leaving a sharp melting peak at 267.2°C, as indicated by the curve (f). With the HDB in the spinning process, the spun fibers, as indicated by (b), (c), and (d), possess no more than 26.3% crys-

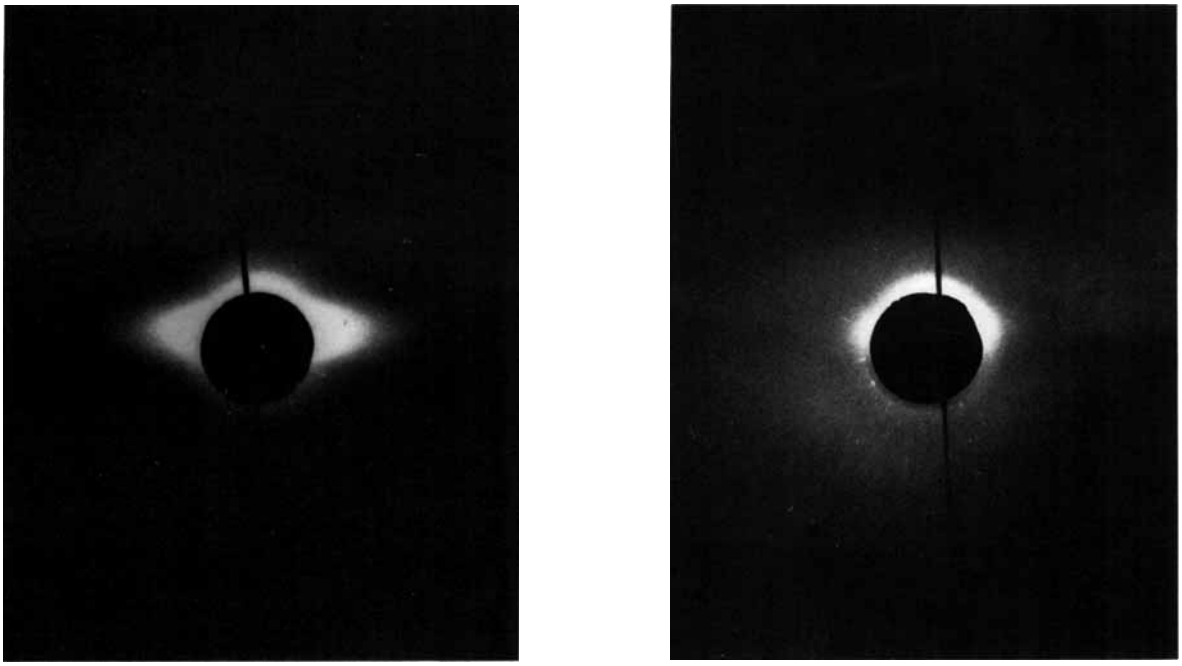

(a) (b)

Figure 21 SAXS patterns of PET filaments obtained at various conditions: (a) 4000 m/min take-up with TCZ (250°C) and HDB (110°C and 28 cm); (b) 3250 m/min take-up with HDB (150°C and 28 cm).

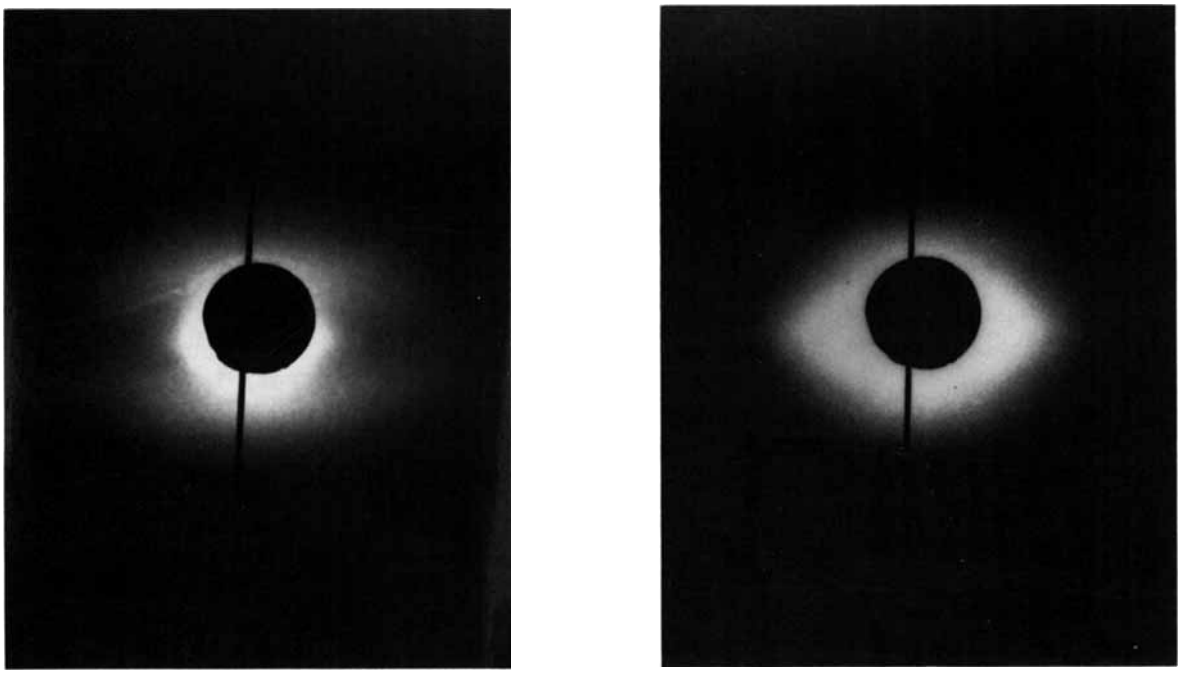

(a) (b)

Figure 22 SAXS patterns of pet filaments obtained at various conditions: (a) 4250 m/min take-up with HDB (180°C and 12 cm); (b) 6000 m/min take-up with TCZ (250°C).

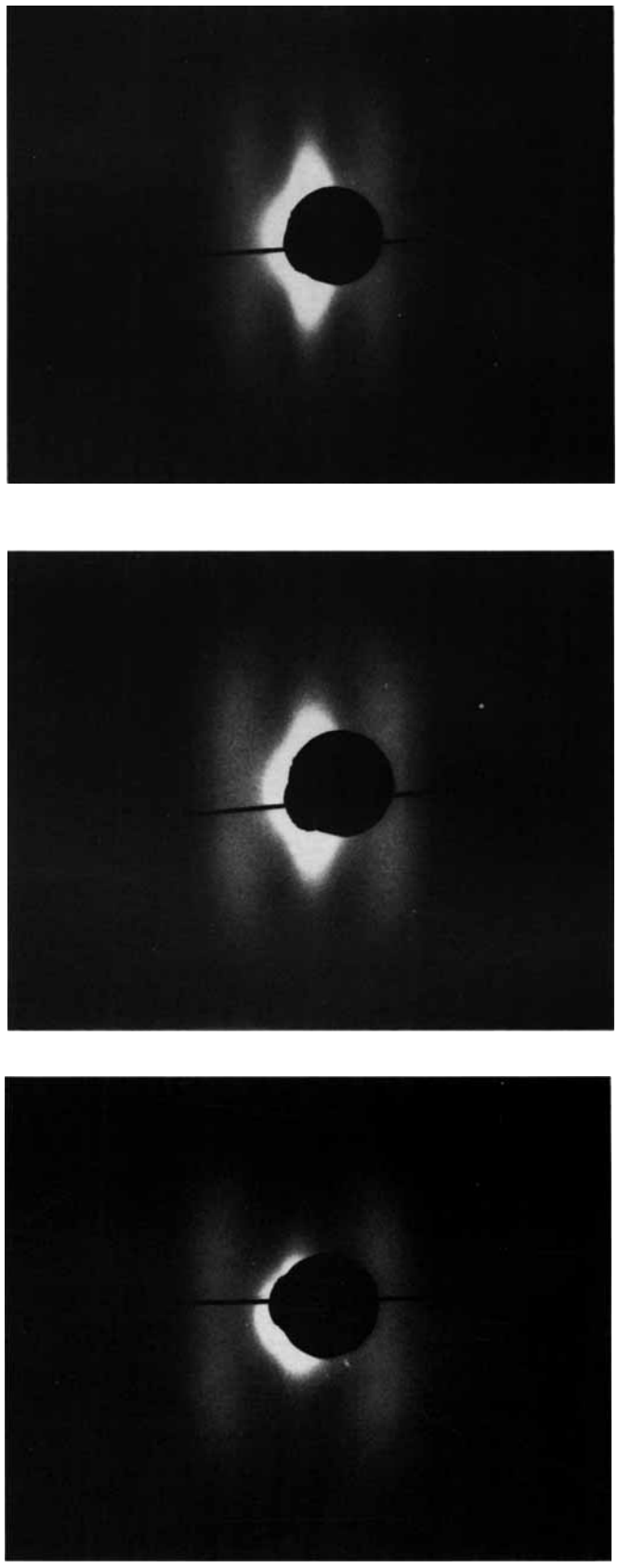

Figure 23 SAXS patterns of annealed (195°C and 5 min) PET filaments obtained at various conditions: (a) 5500 m/min take-up with HDB (25°C and 8 cm); (b) 5500 m/min take-up with TCZ (250°C) and HDB (95°C and 32 cm); (c) 4000 m/min take-up with TCZ (250°C) and HDB (110°C and 28 cm).

tallinity. However, it is surprising that the exotherm crystallization peaks are not as obvious as in the case of curve (a). This further supports the presumption made earlier that fibers spun under the HDB process possess a rich oriented mesophase, which might not be able to crystallize during the heating process. Moreover, the melting peaks are sharper than those of the high-speed spun fibers with melting points, respectively, of 252.7, 254.6, and 254.3°C for curves (b), (c), and (d). The respective narrow melting peaks and lower melting points represent low crystallinity and small crystallite size present in the fibers. With an increase of the HDB temperature to 180°C, the fibers spun have high crystallinity, 43.1%. However, the melting point, 258.9°C, as shown by diagram (e), is still lower, and the melting peak is sharper than that of high-speed spun fibers, shown in diagram (f). This indicates that even though fibers of high crystallinity can be obtained from the higher HDB temperature, the crystallite size is still smaller.

WAXS-azimuthal scans were used to determine the crystalline orientation factor. Additionally, with the birefringence methods, the amorphous orientation was then calculated. Since there is no satisfactory model or method leading to the separation of mesophase from the amorphous phase, the calculation is based on a two-phase model without concern for the mesophase. Therefore, the resulting amorphous orientation factor involves the contribution from "pure" amorphous phase and mesophase. Figure 20 shows the change of crystalline orientation factors f_c and amorphous orientation factor f_a with take-up speed at different HDB temperatures. The f_c is a decreasing function of take-up speed while f_a is a monotonically increasing function. This suggests that the small crystals formed at high take-up speed are less oriented than the mixture of amorphous phase and mesophase. Unlike the structural formation mechanism of conventional high-speed spinning, it is suspected that under extremely high spinning stress the majority of molecular chains are preferentially oriented to form the mesophase with slightly less constrained molecular chains to form the crystalline phase. In other words, during the HDB spinning process, the molecular chains, which bear less stress as well as less strain, in the fiber can gain a certain degree of rotational freedom to join the crystalline lattice while the load-bearing molecular chains are further oriented and extended to form the mesophase. The evidence can be seen in the tendency of f_a to increase with the increase of take-up speed. Increase of HDB temperature helps induce the thermal mobility of molecular chains, as opposed to the constraint from high spinning stress, to transform the structure into a crystalline lattice. Fibers produced from the spinning process with the use of HDB have a high f_a, very close to that of the spin–draw process, and this is considered to be the main factor responsible for the superior mechanical properties although f_c is inferior compared with that of high-speed spun fibers.

Figure 21(a) shows typical SAXS patterns of fibers spun via the HDB at temperature below 110°C. Scattering in the meridional direction cannot be clearly seen. It is reasoned that too small crystallite sizes and the less precisely defined inhomogeneity or periodicity in the fiber direction are responsible for the weak scattering in SAXS patterns. Gradually, a faint scattering starts to emerge when the HDB

Table IV Comparison of Long Period Spacing (LSP) and Crystalline Dimension of PET (IV = 0.95) Spun Fibers under Various Post Treatment Conditions

Speed (m/min)	TCZ (°C)	HDB Length (cm)	HDB Temperature (°C)	State	LPS (Å)	$L_{\bar{1}05}$ (Å)	$L_{\bar{1}05}$/LPS (%)	Note
5500	None	8	25	Annealed	117	46.3	39.4	1
5000	250	32	95	Annealed	135	47.4	35.1	1
4000	250	28	110	Annealed	145	54.2	37.4	1, 2
3250	None	28	150	As-spun	154	50.6	32.8	—
4250	None	12	180	As-spun	159	63.2	39.8	—
3500	250	28	110	Drawn and annealed	149	44.2	29.6	3
6000	250	None	None	As-spun	143	76.5	53.5	—
Spun–drawn	—	—	—	—	162	63.2	39.1	—

Note: (1) Annealing conditions: 5 min at 195°C in air circulating oven under constant length; (2) 4.5 dpf at as-spun; (3) drawing and annealing condition: Preheat roll: 90°C; hot plate: 250°C, 10 in.; draw ratio: 1.2; take-up speed: 10 m/min.

is increased up to 150°C as shown in Figure 21(b). Clear reflection of two meridional streaks can be seen when the HDB is further increased to 180°C, as shown in Figure 22(a), as opposed to the two-spot reflection of high-speed spun fibers as shown in Figure 22(b). Vassilatos et al.[29] explained that the meridional streak is indicative of a group of oriented fibrils composed of crystals at a periodic distance of long period spacing (LPS).

Four-spot SAXS patterns were developed after the annealing of fibers at 195°C for 5 min as shown in Figure 23. Prior to heat treatment, the patterns are typically shown as in Figure 21(a). The four-spot SAXS patterns are indicative of a checkerboard pattern of skewed crystals. LPS derived from the

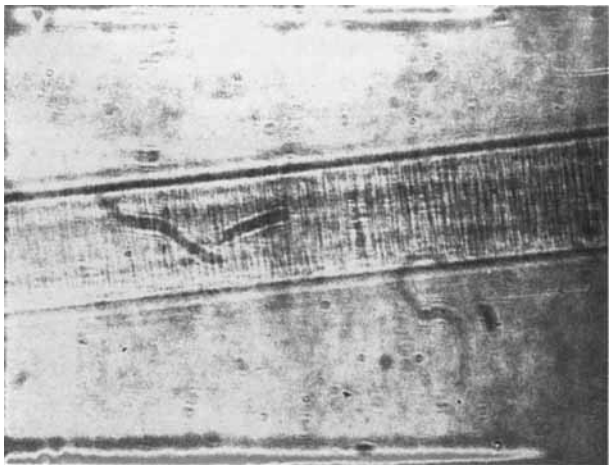

(a)

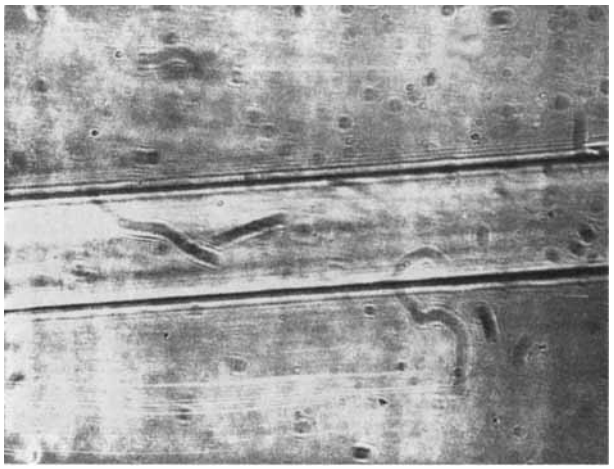

(b)

Figure 24 Photomicrograph of PET filaments: (a) containing transverse lines; (b) transverse lines disappear upon drawing and annealing.

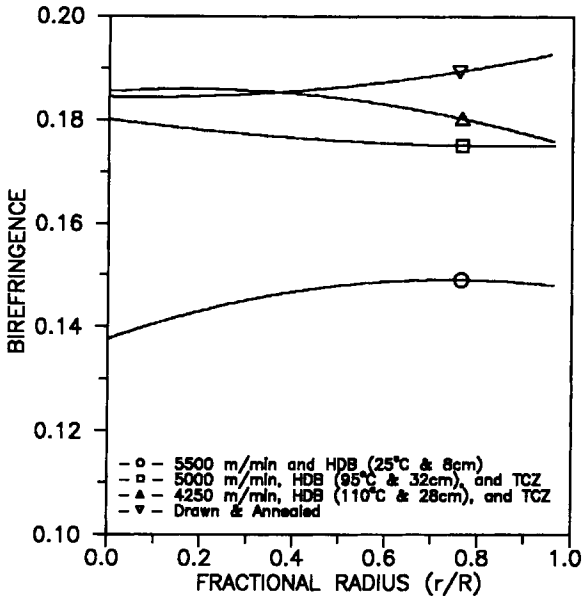

Figure 25 Radial distribution of birefringence of PET (IV = 0.95) fibers spun under different conditions.

separation of scattering patterns of various fibers spun under different conditions, along with fibers from the posttreatment, are shown in Table IV. The crystalline dimensions in the direction of the ($\bar{1}05$) reflection plane are included. Moreover, from the calculation of the fraction of crystalline dimension in the LPS (crystallite size/LPS), the fibers spun with the HDB at 180°C have a slightly higher fraction than that of the spun–drawn fibers, but the fraction is still far lower than that of the high-speed spun fibers.

Unique phenomena of fibers spun under varied HDB conditions are that the fibers often show an increase of whiteness in appearance and exhibit many transverse lines when viewed under the microscope as shown in Figure 24(a). This appearance is similar to the phenomenon reported by Nakano et al.[30] in the study of PET drawn fibers. In our studies the first occurrence of transverse lines appear in the spinning process with the HDB temperature at 95°C, HDB path length of 24 cm path length, and take-up speed of 4000 m/min. When the HDB temperature was increased up to 150°C, the transverse lines disappeared. This observation rules out the speculation that a scorching effect might occur by the use of HDB at high temperature. Further studies revealed that the transverse lines are associated with the increase of birefringence above ca. 0.20 as well as the increase of tenacity above ca. 5.5 gf/d. The transverse lines in this case are not due to microcracks since the transverse lines disappear upon

further drawing and annealing, as shown in Figure 24(b). It is believed that the transverse lines are the result of an optical phenomenon and are probably related to the morphology of high molecular orientation and the small crystallite size.

It has long been realized that the occurrence of radial variation of structure associated with high-speed spinning is related to the temperature and stress distribution in the fiber cross section. Radial variation of structure in the cross section of spun fibers is caused by the rapid quenching and by the increase of stress in the skin layer of threadline, which will consequently yield the differential molecular orientation, and hence the differential crystallization rate in the threadline's cross section. The spinning process with the HDB has proved to be effective in developing a highly oriented and uniform molecular structure in the cross section of the fiber. Figure 25 shows the typical radial birefringence of fibers spun with the HDB under different conditions. In general, the radial variation of birefringence is considered to be small, at most within 0.01 difference between the sheath and the core in the case of the HDB at 25°C. When the HDB temperature is raised above 95°C, the radial distribution of the birefringence essentially becomes "flat." This result supports the presumption that the HDB maintains a good isothermal environment in which the structure can develop under a high level of spinning stress. Figure 26 shows the radial distribution of Lorentz density, an optical measure of crystallinity. The sheath portions of the HDB spun fibers are found to have a slightly higher Lorentz density than does the core. However, the difference, at most 2×10^{-3}, is still smaller compared with that of traditional high-speed spun fibers, 5.5×10^{-3}. Upon further drawing and annealing, the fibers exhibit a high Lorentz density, which is consistent with the increase of crystallinity measured by the density method, and the difference of Lorentz density is reduced to a minimum level. The radial structure characterization suggests that fibers spun under the HDB process possess a uniform distribution of structure in the cross section of the fibers. This situation contributes greatly toward the attainment of the superior mechanical properties of the fibers.

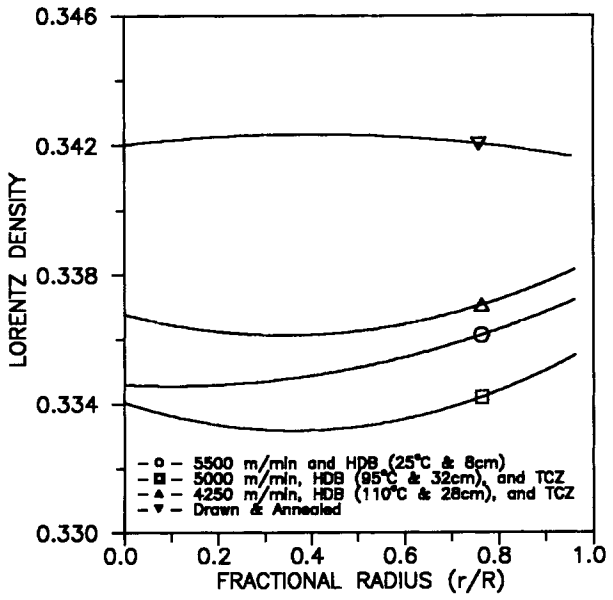

Figure 26 Radial distribution of Lorentz density of PET (IV = 0.95) fibers spun under different conditions.

CONCLUDING REMARKS

It is evident from this work that high spinning stress can be achieved with the introduction of a hydraulic drag bath (HDB) into the threadline of a melt spinning process. The dynamics of spinning are changed from a process controlled by inertia and air drag forces to one controlled by an imposed liquid drag. With the application of HDB, the important factors of temperature, time and tension, which control the structure formation have been uncoupled and optimized during the spinning process. High tensile stress developed in the HDB induces molecular orientation within the spun fibers. The extent of molecular orientation is mainly controlled by the stress and temperature of the filament generated in the HDB. This work contributes a further understanding of structure development under extreme conditions of controlled threadline dynamics.

The authors express their gratitude to the National Science Foundation for financial support, in part, of the project under Grant No. MSM-8417873 and to the Goodyear Tire and Rubber Company for supplying poly(ethylene terephthalate) polymer used in this work.

REFERENCES

1. W. H. Carothers and J. W. Hill, *J. Am. Chem. Soc.*, **54,** 1579 (1932).
2. A. Ziabicki and K. Kedzierska, *J. Appl. Polym. Sci.*, **6,** 111 (1962).
3. J. H. Dumbleton, *Textile Res. J.*, **40,** 1035 (1970).
4. K. Nakamura, K. Katayama, and T. Amano, *J. Appl. Polym. Sci.*, **17,** 1031 (1973).
5. J. Shimizu, K. Toriumi, and Y. Imai, *Sen-i Gakkaishi,* **33,** T-255 (1977).

6. H. M. Heuvel and R. Huisman, *J. Appl. Polym. Sci.*, **22,** 2229 (1978).
7. G. Perez and C. Lecluse, International Man-Made Fibers Conference, Dornbirn, Austria, 1979.
8. A. Ziabicki and H. Kawai (Eds.), *High Speed Fiber Spinning,* Wiley, New York, 1985.
9. J. A. Cuculo, P. A. Tucker, G. Y. Chen, C. Y. Lin, and J. Denton, *Intern. Polym. Processing,* **4,** 85 (1989).
10. Cuculo et al., U.S. Pat. 4,909,976.
11. D. W. Ihm and J. A. Cuculo, *J. Polym. Sci. Polym. Phys. Ed.,* **25,** 619 (1987).
12. S. K. Garg, *J. Appl. Polym. Sci.,* **29,** 2111 (1984).
13. M. Matsui, *Trans. Soc. Rheol.,* **20,** 465 (1976).
14. S. Kase and T. Matsuo, *J. Appl. Polym. Sci., A,* **3,** 2541 (1965).
15. J. Shimizu, N. Okui, and T. Kikutani, in *High-Speed Fiber Spinning,* A. Ziabicki and H. Kawai, Eds., Interscience, New York, 1985, Chap. 7.
16. K. I. Katayama and M. G. Yoon, in *High-Speed Fiber Spinning,* A. Ziabicki and H. Kawai, Eds., Interscience, New York, 1985, Chap. 8.
17. G. Farrow and J. Bagley, *Text. Res. J.,* **32,** 587 (1962).
18. H. M. Heuvel, R. Huisman, and K. C. J. B. Lind, *J. Polym. Sci. Polym. Phys. Ed.,* **14,** 921 (1976).
19. P. Scherrer, *Gottingher Nachrichten,* **2,** 98 (1918).
20. V. B. Gupta and S. Kumar, *J. Polym. Sci. Polym. Phys. Ed.,* **17,** 179 (1979).
21. J. H. Dumbleton, *J. Polym. Sci. Ser. A-2,* **6,** 795 (1968).
22. H. R. E. Frankfort and B. H. Knox, U.S. Pat. 4,134,882 (1979).
23. C. Y. Lin, Ph.D. Dissertation, North Carolina State University, 1990.
24. A. Ziabicki and L. Jarecki, in *High-Speed Fiber Spinning,* A. Ziabicki and H. Kawai, Eds., Interscience, New York, 1985, Chap. 9.
25. J. Shimizu, N. Okui, and T. Kikutain, in *High-Speed Fiber Spinning,* A. Ziabicki and H. Kawai, Eds., Interscience, New York, 1985, Chap. 15.
26. G. Jellinek, W. Ringens, and G. Heidemann, *Ber. Bunsenges. Phys. Chem.,* **20,** 564 (1970).
27. J. Shimizu, T. Kikutani, A. Takaku, and N. Okui, *Sen-i Gakkaishi,* **40,** T-177 (1984).
28. H. H. George, in *High-Speed Fiber Spinning,* A. Ziabicki and H. Kawai, Eds., Interscience, New York, 1985, Chap. 10.
29. G. Vassilatos, B. H. Knox, and H. R. E. Frankfort, in *High-Speed Fiber Spinning,* A. Ziabicki and H. Kawai, Eds., Interscience, New York, 1985, Chap. 14.
30. N. Nakano, M. Kishino, and A. Konda, *Sen-i Gakkaishi,* **26,** 191 (1970).

Received September 25, 1991
Accepted November 11, 1991